Age-related tumor growth in mice is related to integrin α 4 in CD8+ T cells

Juhyun Oh, … , Mikael J. Pittet, Ralph Weissleder

Research Article Aging Immunology

Cancer incidence increases with age, but paradoxically, cancers have been found to grow more quickly in young mice compared with aged ones. The cause of differential tumor growth has been debated and, over time, attributed to faster tumor cell proliferation, decreased tumor cell apoptosis, and/or increased angiogenesis in young animals. Despite major advances in our understanding of tumor immunity over the past 2 decades, little attention has been paid to comparing immune cell populations in young and aged mice. Using mouse colon adenocarcinoma model MC38 implanted in young and mature mice, we show that age substantially influences the number of tumor-infiltrating cytotoxic CD8+ T cells, which control cancer progression. The different tumor growth pace in young and mature mice was abrogated in *RAG1^{null}* mice, which lack mature T and B lymphocytes, and upon selective depletion of endogenous CD8+ cells. Transcriptome analysis further indicated that young mice have decreased levels of the *Itga4* gene (CD49d, VLA-4) in tumor-infiltrating lymphocytes when compared with mature mice. Hypothesizing that VLA-4 can have a tumor-protective effect, we depleted the protein, which resulted in accelerated tumor growth in mature mice. These observations may explain the paradoxical growth rates observed in murine cancers, point to the central role of VLA-4 in controlling tumor growth, and open new venues to therapeutic manipulation.

Find the latest version:

Age-related tumor growth in mice is related to integrin α4 in CD8+ T cells

Juhyun Oh,[1] Angela Magnuson,[2] Christophe Benoist,[2] Mikael J. Pittet,[1] and Ralph Weissleder[1,3]

[1]Center for Systems Biology, Massachusetts General Hospital (MGH), Boston, Massachusetts, USA. [2]Division of Immunology, Department of Microbiology and Immunobiology, Harvard Medical School and Evergrande Center for Immunologic Diseases, Harvard Medical School and Brigham and Women's Hospital, Boston, Massachusetts, USA. [3]Department of Systems Biology, Harvard Medical School, Boston, Massachusetts, USA.

Cancer incidence increases with age, but paradoxically, cancers have been found to grow more quickly in young mice compared with aged ones. The cause of differential tumor growth has been debated and, over time, attributed to faster tumor cell proliferation, decreased tumor cell apoptosis, and/or increased angiogenesis in young animals. Despite major advances in our understanding of tumor immunity over the past 2 decades, little attention has been paid to comparing immune cell populations in young and aged mice. Using mouse colon adenocarcinoma model MC38 implanted in young and mature mice, we show that age substantially influences the number of tumor-infiltrating cytotoxic CD8+ T cells, which control cancer progression. The different tumor growth pace in young and mature mice was abrogated in *RAG1^null* mice, which lack mature T and B lymphocytes, and upon selective depletion of endogenous CD8+ cells. Transcriptome analysis further indicated that young mice have decreased levels of the *Itga4* gene (CD49d, VLA-4) in tumor-infiltrating lymphocytes when compared with mature mice. Hypothesizing that VLA-4 can have a tumor-protective effect, we depleted the protein, which resulted in accelerated tumor growth in mature mice. These observations may explain the paradoxical growth rates observed in murine cancers, point to the central role of VLA-4 in controlling tumor growth, and open new venues to therapeutic manipulation.

Introduction

Solid cancers are primarily a disease of adults, with roughly 95% of new cases occurring after the age of 40 (1). Paradoxically, it has been reported that tumors grow considerably faster at a young age in both humans and mice (2–4). For example, bronchogenic, breast, and colon cancer has been reported to grow more rapidly in young patients (5–7). Previous reports have attributed this age-related difference to faster cell proliferation, decreased tumor cell apoptosis (8), and increased angiogenesis in young animals (3, 4). Additionally, early studies of BM transfusion suggested that the immune system might play a role in retarded tumor growth in aged mice (9). However, individual immune cell populations have not been compared in detail in young and aged mice, despite the major advances in understanding antitumor immunity over the past 2 decades. We reasoned that investigating immune aspects of this paradoxical growth could shed light on immune cell function and aging, perhaps with therapeutic consequences.

The immune system is an effective, protective physiological system in mammals. Both the innate and adaptive branches of the immune system are susceptible to age-related changes (immunosenescence) (10–12). Overall, T cell numbers decline with age as thymic involution leads to decreased cellular output. With dwindling thymic T cell production, homeostatic proliferation of peripheral T cells is responsible for maintaining naive T cell numbers. While this may initially be an effective mechanism, it eventually fails, resulting in fewer naive T cells and allowing memory and effector T cells to become dominant (13, 14). In addition to the numerical decline, T cell receptor (TCR) repertoire diversity progressively contracts over time (13–15), thus further skewing T cell responses. As the immune system is important in controlling cancer, dysfunctional immunity in the elderly may compromise immunosurveillance, thereby fueling cancer growth in the adult. These observations, however, do not explain the faster tumor growth rates in young mice.

Given the paradoxical tumor growth/immune axis, we investigated tumor-infiltrating immune cell populations in young and older, mature mice. Studying natural responders and elite controllers could be

an extraordinarily powerful way to understand how the immune systems controls some cancers. Using the immunocompetent MC38 and other models, we observed that tumor growth is indeed accelerated in young mice and delayed in mature mice, an effect that was directly related to the number of infiltrating cytotoxic CD8+ T cells in a given tumor. MC38 is a cancer cell line derived from colon adenocarcinoma in C57BL/6 mice. High immunogenicity of implanted MC38 tumors has provided a good model to investigate tumor-associated immune responses (16). In humans, the incidence of colon and rectal cancer greatly increases in the 5th and 6th decade in both men and women (1). It has been reported that 89% of all colorectal diagnoses are in people older than age 50, and colorectal cancer has been the second leading cause of cancer death in males older than age 40 (17). As we observed in the MC38 model, colon cancer in humans also grows faster in young patients (7).

The different tumor growth effects we observed in young and mature mice were completely eliminated in the *RAG1*null mice, which lack mature T and B lymphocytes. Transcriptome analysis on the tumor-infiltrating immune cell populations indicated much lower levels of the *Itga4* gene (CD49d, VLA-4) in tumoral lymphocytes of young mice. Cytometry confirmed these results. Hypothesizing that VLA-4 had a naturally controlling tumor-protective effect, we depleted the protein, resulting in accelerated tumor growth curves in aged mice. These observations may explain the paradoxical growth rates observed in murine cancers and support VLA-4's central role in controlling tumor growth.

Results

Tumors grow faster in young C57BL/6 mice. A number of previous studies showed that tumor growth rates differ in young and aged mice (2–4). To determine the growth rates in immunocompetent tumor models, we implanted 1×10^6 murine colon cancer (MC38) cells into young (3–4 months old) and mature (12–15 months old) C57BL/6 mice and monitored tumor volumes over time. Older, mature adult mice were 12–15 months of age, which is equivalent to about 45 years in humans (i.e., an age where the rate of cancer incidence increases and the onset of aging phenotype arises in multiple systems, including the immune system; refs. 1, 18–23). As can be seen in Figure 1A, the 2 cohorts had significantly different growth rates (Supplemental Figure 1A). When the tumors were harvested at day 30, the differences were statistically significant ($P < 0.001$; volume of young mice (Vol_{Young}), 786.5 mm³; Vol_{Aged}, 105.3 mm³). We also used B16 melanoma and 4T1 breast cancer models, which are also widely used mouse cancer models, to study the impact of aging on tumor control across multiple tumor models. Similar results were also obtained in the B16 and the 4T1 models (Figure 1, B and C, and Supplemental Figure 1, B and C). These results corroborate older observations from larger cohorts and immunocompetent mouse models (2–4, 8, 9, 24).

Age-related growth differences are abrogated in RAG1null mice. Ershler et al. have reported that this age-dependent difference in tumor growth was able to be reversed by old-to-young BM transplantation, providing evidence that the immune system plays a role in the age-related difference in tumor growth (9). To determine whether the observed differences in growth rates could be explained by immune cell effects, we repeated the above experiments in different mouse models (Figure 1, D–F). The growth differences between tumors in young and mature mice were nullified in *RAG1*null mice, which lack mature B and T lymphocytes (Figure 1D and Supplemental Figure 1D). Indeed, MC38 tumors grew at an accelerated rate in mature *RAG1*null mice, similar to that observed in young immunocompetent C57BL/6 mice. These results were confirmed in the NOD-*scid* IL2Rgnull (NSG) mice, which lack NK cells as well as T and B cells. In these mice, MC38 tumor growth rate was similar in young and mature mice (Figure 1E). Similar results were also seen with B16 melanoma in RAG1null mice (Figure 1F and Supplemental Figure 1E). Given this strong phenotype of tumor growth difference between young and mature immunocompetent mice and the lack thereof in immunocompromised models, we concluded that tumoral immune cells likely play a role.

Immune cell densities change in tumors. To profile the different tumor-associated immune cells, we implanted MC38 tumors into C57BL/6 mice; sacrificed cohorts of mice after 7, 14 or 21 days; excised tumors; and determined tumoral immune cell populations by flow cytometry. These time points were chosen to sample tumor volume differences across the spectrum (day 7, earliest time point when tumor sizes start to diverge between young and mature mice; day 14, divergent growth rates; day 21, late stage tumors). The data are summarized in Table 1 and are shown as single animal figures in Figure 2, A–F. The biggest difference in immune cell populations was observed in CD8+ T cells (Figure 2A). At day 7 ($P = 0.02$) and 14 ($P = 0.007$), CD8+ T cells were significantly more abundant in tumors of aged mice. This trend continued to day 21 but, at that point, was no longer statistically significant ($P = 0.91$). In order to determine if the differences we
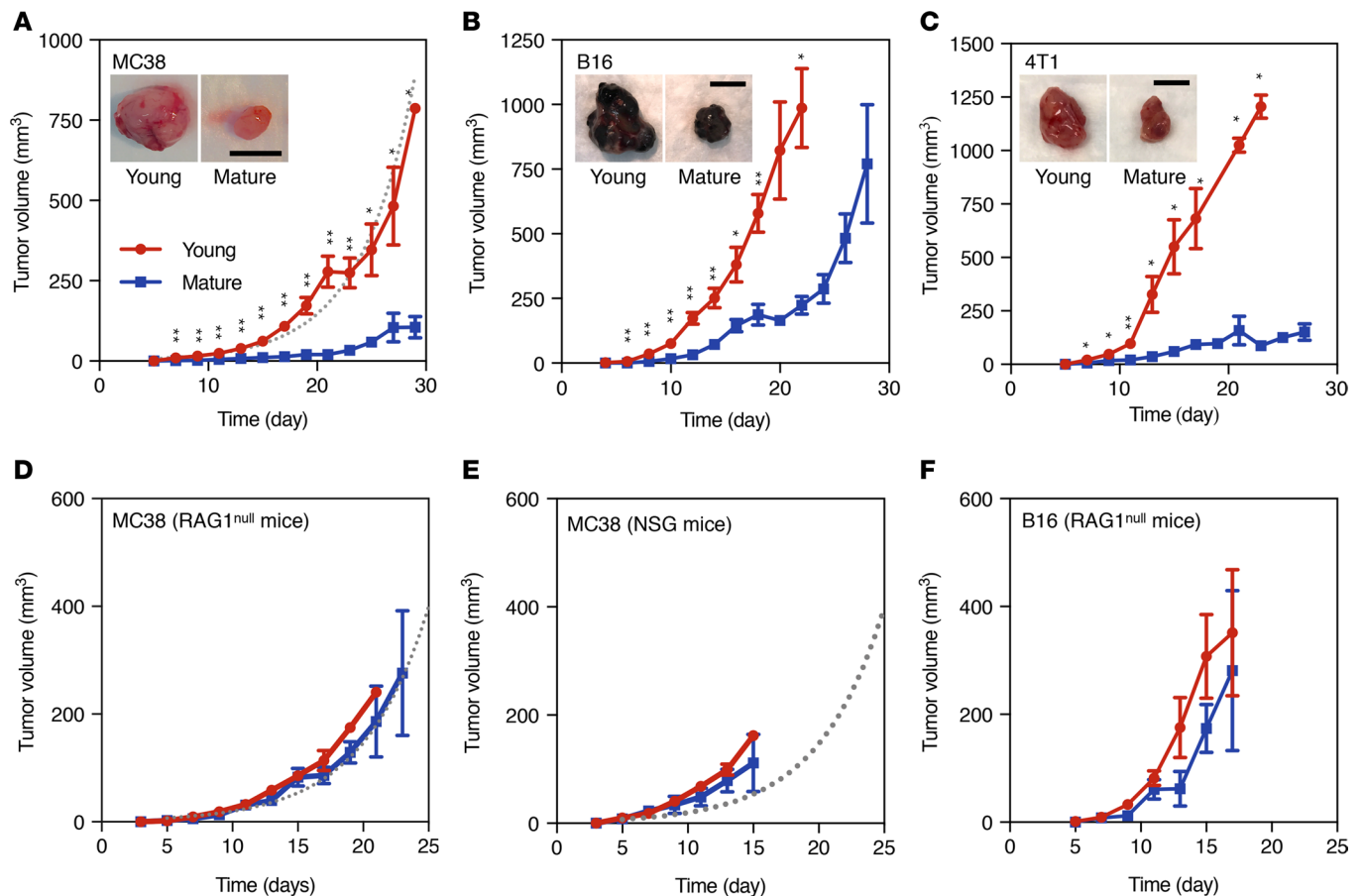
Figure 1. Faster growth rates of murine tumors in young immunocompetent mice are abrogated in *RAG1null* and NSG mice. (**A**) Average growth curves of s.c. MC38 tumors in young (red circle) and mature (blue square) C57BL/6 mice shows accelerated tumor growth in young mice. Dotted line represents the exponential model fit to the tumor size data points from young mice (young mice, *n* = 16; mature mice, *n* = 12). Representative images of MC38 tumors from young and mature hosts at day 30 of tumor growth are shown. (**B**) S.c. B16 tumor growth in young and mature C57BL/6 mice (young, *n* = 7; aged, *n* = 9). Representative images of B16 tumors from young and mature hosts at day 27 of tumor growth are shown. (**C**) S.c. 4T1 tumor growth in young and mature Balb/C mice (*n* = 6 per group). Representative images of 4T1 tumors from young and mature hosts at day 27 of tumor growth are shown. (**D** and **E**) Average growth of MC38 tumor in young (red circle) and mature (blue square) *RAG1null* mice (*n* = 6 each group) (**D**) and NOD-*scid* IL2Rg*null* (NSG) mice (*n* = 5 each group) (**E**) shows no age-dependent difference in tumor growth (*n* = 6 each group). (**F**) B16 tumor growth in young and aged *RAG1null* mice (*n* = 5 each group) also showed no age-dependent difference in tumor growth. All data are plotted as means ± SEM. *P* values were calculated using the Mann-Whitney *U* test (*$P < 0.05$, **$P < 0.005$). Scale bars: 1 cm.

see in immune cell count are affected by different sizes of tumors of young and mature mice, we compared CD8+ T cell counts in tumors of similar sizes from young and mature animals. For example, 21-day tumors in mature mice are similar in volume to 7-day tumors in young mice; however, the CD8+ T cell counts were approximately 30-fold higher in 21-day tumors in aged mice (Figure 2F, *P* = 0.001). By comparing the number of tumor-infiltrating CD8+ T cells in tumors grown to the similar size in young and mature mice (although at different time points of tumor harvest), Figure 2F corroborates that the increased CD8+ T cell infiltration in tumors is an age-associated phenotype.

There were also differences in other cell types, including CD4+ T cell (high in mature, Figure 2B), tumor-associated macrophage (TAM, high in the tumors of mature mice, Figure 2D), and DC (high in mature, Figure 2E). However, compared with CD8+ T cell, these differences were typically less pronounced and did not carry across multiple time points. Finally, the CD8+ T cell/Treg ratios were generally much higher in tumors of mature mice (Table 1). Since the tumoral CD8+ T cell counts were dramatically different in tumors, we also compared lymphocyte levels in lymphoid organs from the same mice (i.e., we profiled the lymphocyte numbers in spleens and peripheral blood from tumor-bearing mice). As can be seen in Table 1, splenic and peripheral blood lymphocyte levels did not show statistically significant differences between young and mature mice.

Table 1. Overview of immune cell content in MC38 tumors, spleen, and peripheral blood in young and mature mice

	No. of cells/mg	Day 7			Day 14		
		Young (n = 9)	Mature (n = 11)	P value	Young (n = 18)	Mature (n = 18)	P value
Tumor	Weight (mg)	61.5 ± 9.6	29.7 ± 5.1	0.007	112.1 ± 21.0	49.9 ± 9.9	0.01
	CD8+ T cell	58.5 ± 16.7	145.0 ± 27.3	0.02	410.9 ± 60.8	1280.2 ± 345.7	0.007
	CD4+ T cell	167.1 ± 61.1	170.40 ± 44.8	0.8	243.8 ± 80.4	1059.2 ± 268.1	0.01
	CD25+ CD4+	67.6 ± 25.4	37.5 ± 11.7	0.5	341.2 ± 66.5	427.0 ± 95.3	0.68
	Treg	21.2 ± 4.9	12.9 ± 2.9	0.3	24.1 ± 7.5	34.2 ± 1.7	0.63
	Macrophage	1228.1 ± 286.6	1793.22 ± 457.2	0.2	922.4 ± 189.3	2451.9 ± 492.8	0.02
	DC	189.4 ± 71.2	242.4 ± 88.6	0.3	193.4 ± 60.6	900.8 ± 188.2	0.02
	CD103+ DC	12.1 ± 2.9	14.0 ± 3.1	0.7	8.2 ± 0.1	9.4 ± 0.14	0.37
	CD8/Treg ratio	2.76 ± 1.16	12.34 ± 4.89	0.01	17.05 ± 5.97	37.63 ± 11.60	0.01
	CD8/TAM ratio	0.05 ± 0.02	0.07 ± 0.02	0.07	0.29 ± 0.13	0.52 ± 0.31	0.7
	CD8/DC ratio	0.31 ± 0.15	0.60 ± 0.38	0.08	2.12 ± 1.43	1.42 ± 0.86	0.8
Spleen	Weight (mg)	79.8 ± 2.7	127.3 ± 1.4	0.002	159.8 ± 24.0	162.7 ± 21.1	0.9
	CD8+ T cell	9920.5 ± 867.8	8384.6 ± 897.9	0.2	9904.7 ± 563.1	9423.6 ± 754.8	0.6
	CD4+ T cell	14263.2 ± 1339.7	13049 ± 1117.5	0.5	14337.6 ± 947.0	14105.7 ± 960.4	0.9
	CD11b+ F4/80+	467.8 ± 101.6	502.2 ± 59.7	0.8	451.1 ± 67.8	863.3 ± 30.8	0.3
	CD11c+	489.3 ± 84.8	875.8 ± 185.0	0.09	581.3 ± 149.1	1120.3 ± 341.4	0.06
	No. of cells/μl	Young (n = 5)	Mature (n = 5)	P value			
Blood	CD8+ T cell	242.2 ± 11.1	189.7 ± 18.9	0.1			
	CD4+ T cell	285.6 ± 61.5	223.6 ± 82.6	0.5			
	CD11b+ F4/80+	102.9 ± 9.5	204.0 ± 75.9	0.2			
	CD11c+	69.6 ± 27.8	36.2 ± 3.5	0.2			

Immune cell numbers in digested tumors tissues, spleens, and whole blood of tumor-bearing mice at day 7 and day 14 after implantation of 1×10^6 MC38 tumor cells. Cell numbers are adjusted to weight (cells/mg). For cell count in peripheral blood, blood was drawn by heart puncture and the cell numbers are normalized to the volume of blood drawn (cells/μl). For statistical test, t test (2-tailed) was used with correction for multiple comparisons by Holm-Sidak method.

CD8 depletion accelerates tumor growth. Given the notable differences in CD8+ T cell counts, we sought to explore whether CD8 depletion would be sufficient to alter tumor growth rates. Using cohorts of C57BL/6 mice, we implanted MC38 tumor cells on day 0 and then treated animals with anti-CD8 antibody injections or control IgG isotype (25 μg/g body weight, i.p. injection) every other day until tumor harvest (Supplemental Figure 2A). At the end of the study, tumors were harvested and processed for flow cytometry. CD8 depletion was efficient in both young and aged mice. On average, the CD8+ T cell pool was depleted by about 80%–90% (Supplemental Figure 2, B and C). The CD8 depletion had a larger effect in tumors growing in mature mice; upon CD8 depletion, tumor growth rates in mature mice became indistinguishable from those observed in young animals (Figure 2, G–I). These results indicate that CD8+ T cells likely play a dominant role in tumoral growth rates.

Transcriptome analysis of tumoral T cells reveals the importance of Itga4. To further investigate molecular drivers on T cells, we performed transcriptome analysis of different T cell subsets in young and aged mice (Figure 3, A–C). Cohorts of young and mature mice bearing MC38 tumors were sacrificed, tumors were harvested at day 10, and T cells were sorted to high purity and processed for gene expression profiling by RNA sequencing (RNA-seq). Figure 3, A–C, shows the top up- and downregulated genes in these cohorts (FDR < 0.05). Of interest was *Itga4*, which emerged as a marker that was upregulated in all 3 profiled T cell subsets of mature mice (CD8+, CD4+, and Treg). Integrin subunit α 4 (ITGA4; CD49d) forms a heterodimer with integrin β 1 (ITGB1; CD29) in the α4β1 lymphocyte homing receptor (also referred to as VLA-4). *Itga4* gene was expressed at much lower levels in tumoral T cells of young animals compared with mature ones. Given that the results point to a strong connection between CD8+ T cell infiltration and *Itga4* expression in tumoral lymphocytes, we also determined the expression level of ITGA4 (CD49d) in tumoral, splenic, and peripheral lymphocytes in young and mature mice by flow cytometry (Figure 3, D–F, and Supplemental Figure 3). Tumoral CD8+ T cells of mature mice showed significantly higher CD49dhi cell frequency and CD49d mean fluorescence
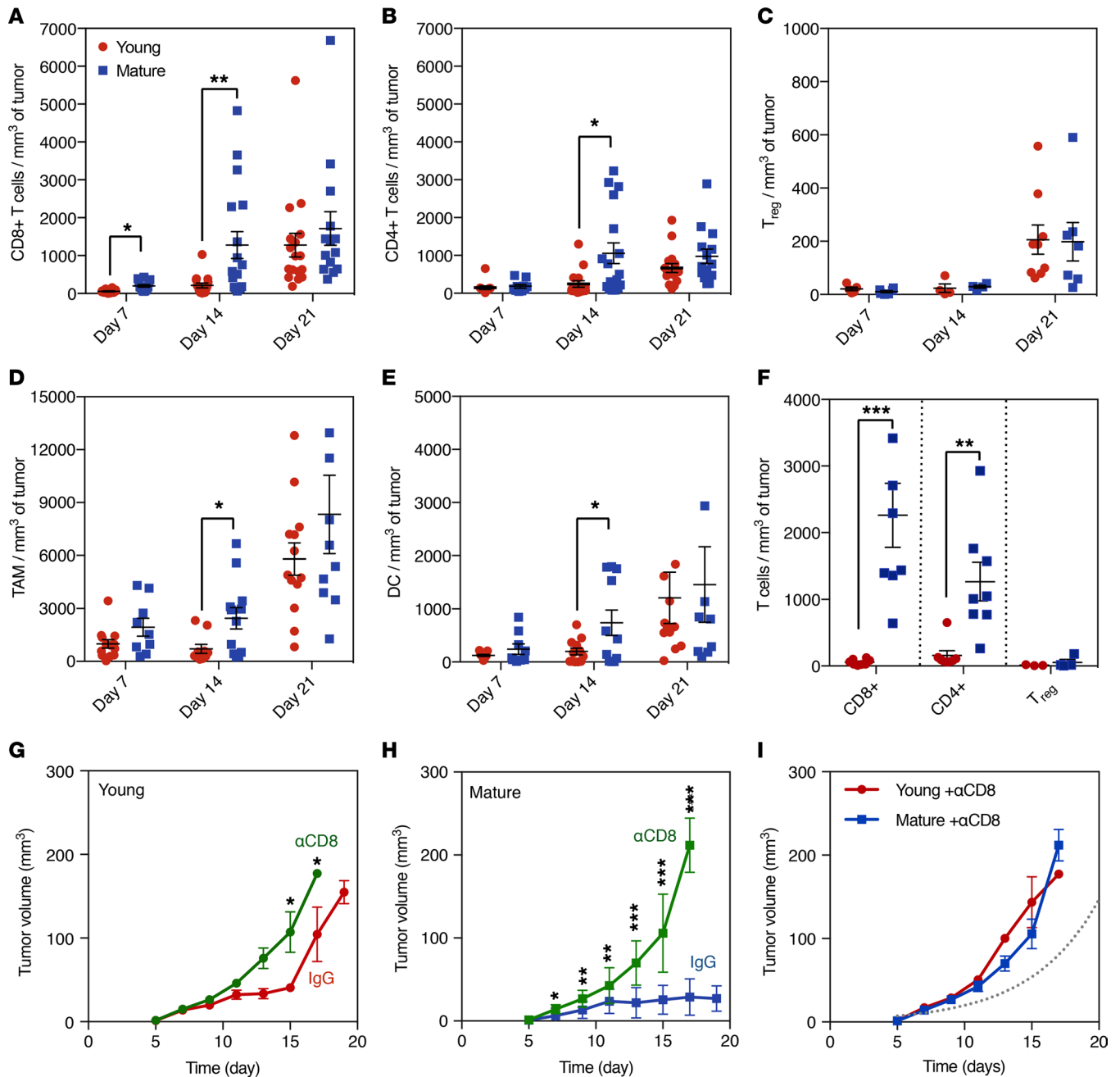
Figure 2. Increased CD8⁺ T cell infiltration controls MC38 tumor growth in mature mice. Numbers of tumor-infiltrating cells per mm³ of tumor tissue counted at days 7, 14, and 21 of tumor growth show changes in immune infiltration over time. (**A**) CD8⁺ T cell (CD45⁺TCRβ⁺CD8⁺; day7: young *n* = 7 (red circle), mature *n* = 11 (blue square); day 14: *n* = 18 per group; day 21: young *n* = 17, mature *n* = 14). (**B**) CD4⁺ T cell (CD45⁺TCRβ⁺CD4⁺; day7: young *n* = 7, mature *n* = 11; day 14: *n* = 18 per group; day 21: young *n* = 17, mature *n* = 14). (**C**) Treg (CD45⁺TCRβ⁺CD4⁺CD25⁺FoxP3⁺; day7: *n* = 6 per group; day 14: *n* = 5 per group; day 21: young *n* = 9, mature *n* = 5). (**D**) Tumor-associated macrophage (CD45⁺CD11b⁺F4/80⁺MHCII⁺; day7: *n* = 10 per group; day 14: *n* = 16 per group; day 21: young *n* = 13, mature *n* = 10). (**E**) DC (CD45⁺CD11c⁺MHCII^hi; day7: *n* = 9 per group; day 14: *n* = 11 per group; day 21: young *n* = 13, mature *n* = 9). (**F**) Tumors of similar sizes (40–50 mm³) from young and mature mice (at different time points of tumor growth) were compared for T cell counts per unit volume of tumor tissues. (**G**) MC38 tumor growth in young mice treated with anti-CD8 antibody (green circle) or IgG isotype control antibody (red circle; *n* = 9 per group). (**H**) MC38 tumor growth in aged mice treated with anti-CD8 antibody (green square) or IgG isotype control (blue square; *n* = 6 per group). (**I**) Superimposed MC38 tumor growth curves of young and mature mice with CD8 depletion shows that CD8 depletion eliminates age-dependent differences in tumor growth rate. Dotted line shows the exponential model fit to the tumor size data points of young C57BL/6 mice from Figure 1A. All data are plotted as means ± SEM. For statistical test, *t* test (2-tailed) was used with correction for multiple comparisons by Holm-Sidak method (*$P < 0.05$, **$P < 0.005$, ***$P < 0.0005$).
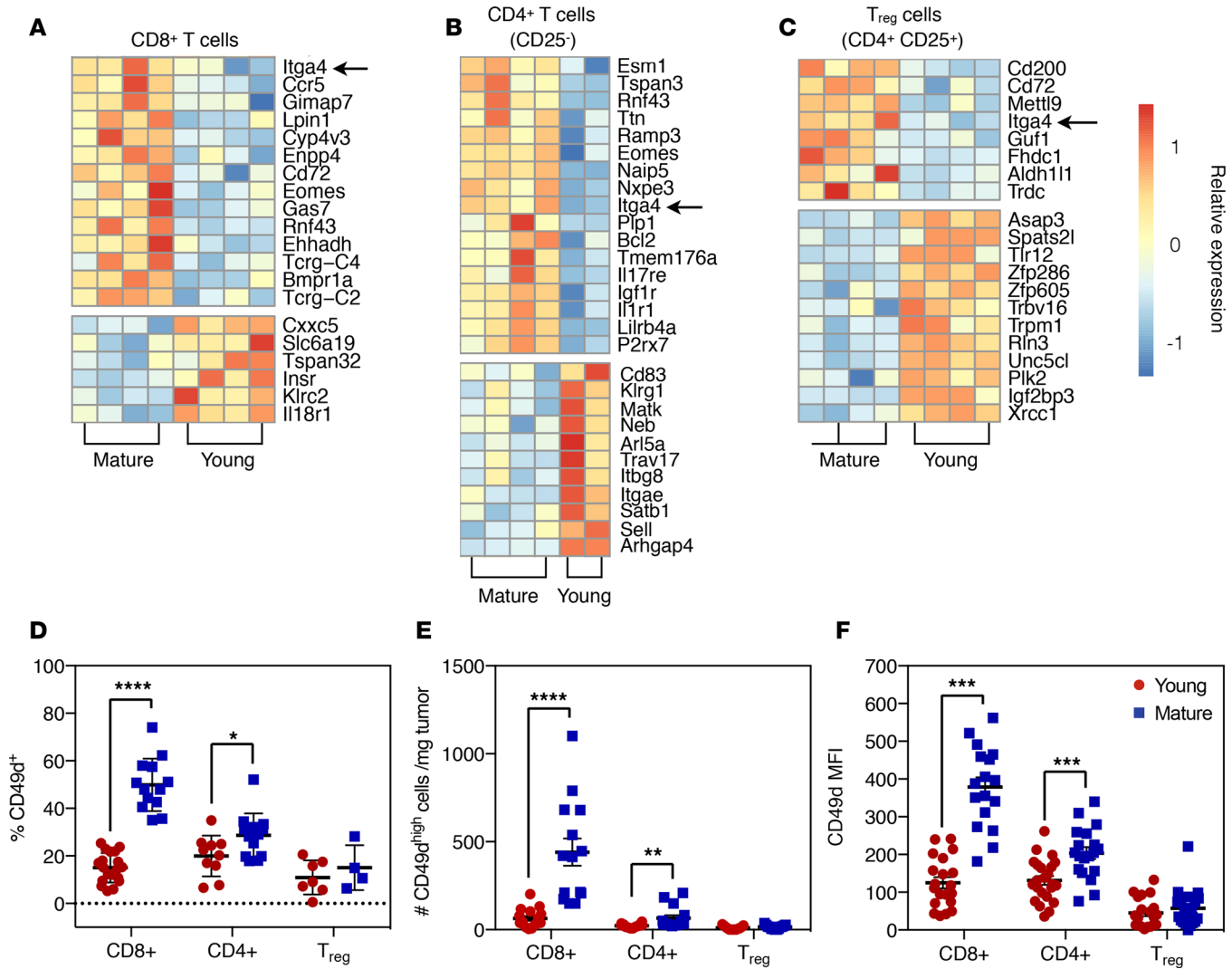
Figure 3. Transcriptome analysis reveals age-dependent upregulation of ITGA4 in tumoral T cells. RNA-seq analysis was performed on double-sorted tumoral T cell populations. (**A**) CD8+ T cell (CD45+TCRβ+CD8+), (**B**) CD4+ T cells (CD45+TCRβ+CD4+CD25−), and (**C**) Treg (CD45+TCRβ+CD4+CD25+). Heatmaps created using the significantly up- and downregulated genes for tumoral CD8+, CD4+, and Treg in comparing young versus mature animals (FDR < 0.05). Each column in heatmaps represents biological replicate. Flow cytometry analysis of ITGA4 (CD49d) expression on CD8+, CD4+, and Treg (CD4+CD25+FoxP3+) cells from tumor tissues of young (red circle) and mature (blue square) mice showed significant increase in the percentage (**D**) and cell count (**E**) of CD49dhi cells among CD8+ and CD4+ T cells. (**F**) Mean fluorescence intensity (MFI) of CD49d confirmed the same trend (n = 15–20 per group). All data in **D–F** are plotted as means ± SEM. For statistical tests in **D**, **E**, and **F**, t test (2-tailed) was used with correction for multiple comparisons by Holm-Sidak method (*P < 0.05, **P < 0.005, ***P < 0.0005, ****P < 0.0001).

intensity compared with tumoral CD8+ T cells of young controls. *Itga4* expression levels in splenic and peripheral lymphocytes of young and mature mice determined by RNA-seq (data not shown) and flow cytometry also showed a tendency toward an age-dependent increase, but the differences were not as prominent nor statistically significant as in tumoral CD8+ T cells (Supplemental Figure 3). Similar observations were made for *Itga4* expression on CD4+ and Treg (Figure 3, D–F, Supplemental Figure 3). We also compared the expression level of the other subunit of VLA-4, ITGB1, in tumoral lymphocytes of young and aged mice. Unlike ITGA4, ITGB1 level remained similar between young and aged mice (Supplemental Figure 4).

CD49dhi CD8+ T cells exhibit elevated cytolytic effector status. In an attempt to understand the function of CD49dhi and CD49dlo CD8+ T cell populations in tumor tissues, we assessed the expression level of various markers (Figure 4, A–D). CD49dhiCD8+ T cells showed significantly higher granzyme B and IFN-γ level than their CD49dlo counterparts, indicating greater cytotoxic potential (Figure 4, A and B). We also assessed the memory phenotype of intratumoral CD49dhi and CD49dlo CD8+ T cell populations.
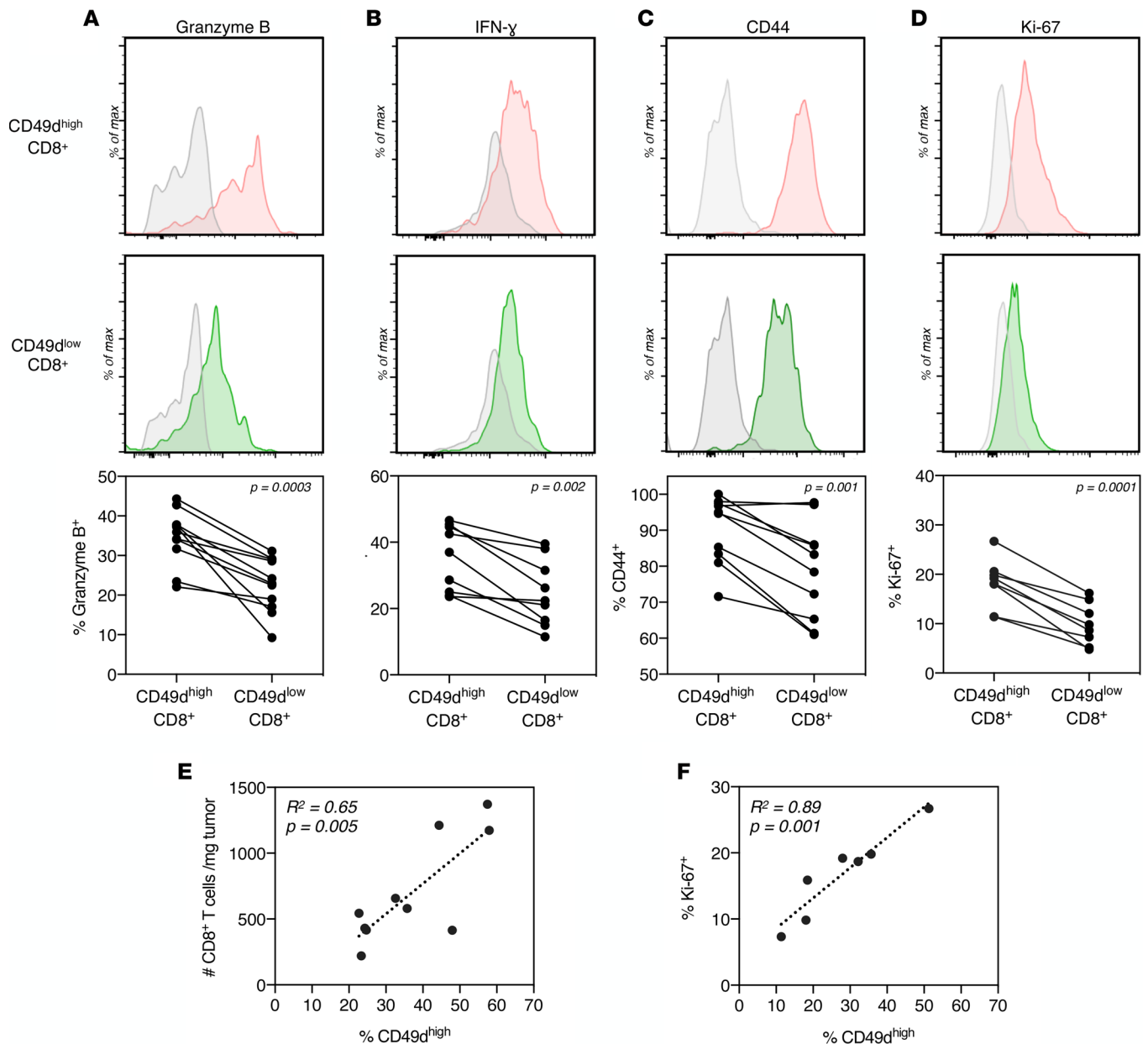
Figure 4. Tumor-infiltrating CD49d^{hi}CD8$^+$ T cells show higher cytotoxic and effector status than CD49d^{lo} cells. S.c. MC38 tumors were harvested on day 14 after implantation and assessed for expression levels of (**A**) granzyme B ($n = 10$), (**B**) IFN-γ ($n = 6$), (**C**) CD44 ($n = 10$), and (**D**) Ki-67 ($n = 7$) in tumor-infiltrating CD49d$^+$ and CD49d$^-$CD8$^+$ T cells of mature mice by flow cytometry. IFN-γ level was measured after restimulation in vitro. Histograms were presented in comparison with unstained controls for granzyme B, CD44, and Ki-67 or with unstimulated control for IFN-γ (gray lines). Each line of before-after graphs represents individual tumors of mature mice. *P* values were calculated based on the 2-tailed paired *t* test between CD49d$^+$ and CD49d$^-$CD8$^+$ T cell subsets in each tumor. (**E**) Linear regression model shows positive correlation between the frequency of CD49d$^+$CD8$^+$ T cells and the number of infiltrating CD8$^+$ T cells. (**F**) Linear regression analysis between the frequency of CD49d$^+$CD8$^+$ T cells and the frequency of Ki-67–expressing CD8$^+$ T cells. Each dot in **E** and **F** represents individual tumor samples of mature mice.

The majority of CD8$^+$ T cells expressed CD44 with higher frequency in CD49d^{hi} than in CD49d^{lo} cells (Figure 4C). A large fraction of CD44$^+$ cells were CD462L$^-$ and CCR7$^-$, showing an effector memory T cell phenotype (Supplemental Figure 5). Measurement of Ki-67 level in intratumoral CD8$^+$ T cells showed higher frequency of proliferating CD49d^{hi} cells than that of CD49d^{lo} counterparts (Figure 4D. Both CD49d^{hi} and CD49d^{lo} CD8$^+$ T cells in tumor express substantial amounts of CD25 and CCR5, which indicates that these T cells are antigen driven (Supplemental Figure 6). There was no statistical difference in the expression level of CD62L, CCR7, CD25, or CCR5 between tumoral CD49d^{hi} and CD49d^{lo} CD8$^+$ T cells of mature mice. The same analysis performed in young mice did not show
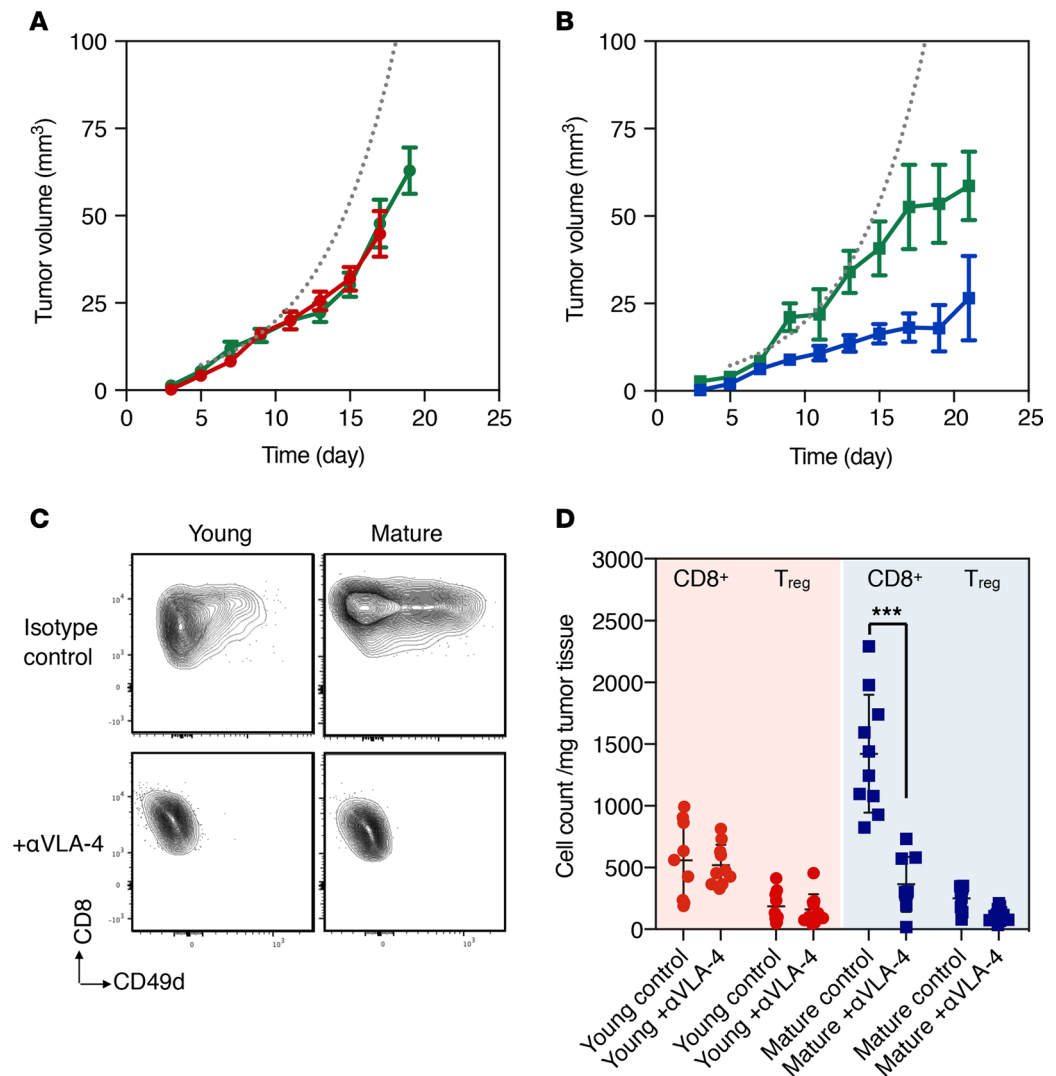
Figure 5. Anti–VLA-4 antibody treatment reverses age-related differences in tumor growth and T cell infiltration frequency. MC38 growth curves of young (**A**) and mature (**B**) mice treated with anti–VLA-4 antibody or IgG isotype control antibody (n = 9 per control group, n = 10 per treatment group). Dotted line shows the exponential model fit to the tumor size data points of young C57BL/6 mice from Figure 1A. Anti-VLA-4 antibody treatment resulted in markedly accelerated tumor growth (**B**) and decreased CD8+ T cell tumor infiltration only in the mature group. (**C**) After anti–VLA-4 antibody treatment, the CD49d expression as measured by flow cytometry was lower in tumoral CD8+ T cells in both young and mature mice. Number of tumor infiltrating T cells were counted (no. cells/mg tumor tissue) and compared among young (red) and mature (blue) mice with or without anti–VAL-4 antibody treatment. (**D**) CD8+ T cell infiltration was significantly reduced in tumors of mature mice that received anti–VLA-4 antibody treatment (young control vs. mature control, P = 0.004; mature control vs. mature +anti–VLA-4, P = 0.0001). For **A**, **B**, and **D**, data are plotted as means ± SEM. P values were calculated using the Mann-Whitney U test for **A–B** and 2-way ANOVA for **D** (***P < 0.001).

prominent differences between tumoral CD49d^hi and CD49d^lo CD8+ T cells, suggesting that CD49d expression is not as important as in tumor-infiltrating CD8+ T cells of mature mice (Supplemental Figure 7).

To further dissect the connection between CD8+ T cell infiltration and CD49d expression in tumoral lymphocytes, we made a direct correlation (Figure 4E). Tumors of mature mice showed a strong correlation between the number of infiltrating CD8+ T cells and the expression level of CD49d in the infiltrating CD8+ T cells (Figure 4D). We also counted and compared the numbers of CD8+ T cells with high and low CD49d level. CD49d^loCD8+ T cells did not show significant difference between 2 age groups, unlike CD49d^hiCD8+ T cells, which exhibited a marked increase in mature group (Figure 3F and Supplemental Figure 8). These data suggest that an increased CD49d^hiCD8+ T cell count in tumors of mature mice accounts for the large part of age-related difference we have seen in CD8+ T cell infiltration. Higher proliferation level of intratumoral CD49d^hiCD8+ T cells of mature mice provides a possible

explanation for the age-dependent increase in CD49d^hiCD8+ T cell number in tumors. In fact, frequency of Ki-67+ cells among CD8+ T cells showed a positive correlation with the frequency of CD49d^hiCD8+ T cells in tumors (Figure 4F).

In addition to T lymphocytes, we observed that TAMs in MC38 tumors also express CD49d. Interestingly, however, CD49d expression in TAMs was similar in young and mature mice (Supplemental Figure 9). Some DCs and a few neutrophils also expressed CD49d, but similar to TAMs, CD49d expression in these cells remained similar in young and mature mice (Supplemental Figure 9). This is in marked contrast to tumor-infiltrating CD8+ T cells, whose percentage expressing CD49d substantially increased in mature mice (Figure 3D, $P < 0.00001$). RNA-seq analysis of TAMs and tumor-infiltrating DCs isolated from tumor tissues of young and mature mice showed minimal to no detectable differences in their transcriptome profiles (Supplemental Figure 9). These data contrast those for T cell populations, which are shown in Figure 3, A–C. We also specifically assessed TAMs in young and mature mice for their expression of representative markers of classically activated (M1) and alternatively activated (M2) markers (Supplemental Figure 9). This analysis further indicated no age-related differences in the polarity of TAMs.

VLA-4 depletion accelerates tumor growth. To test whether VLA-4 modulation would affect tumor growth, we performed in vivo neutralization experiments using an anti–VLA-4 antibody. The experimental design was similar to that of the CD8 depletion experiments shown in Supplemental Figure 2. The impact of anti–VLA-4 treatment is thought to be mediated by blocking the molecular interaction between α4β1-integrin, expressed by lymphocyte and VCAM-1, expressed by vascular endothelial cells (25, 26). Interestingly, anti–VLA-4 treatment had a marked effect on tumor growth in mature mice but not in young mice (Figure 5, A and B). In mature mice, the treatment resulted in accelerated tumor growth that matched the rates seen in young animals. Harvested tumors were also processed for flow cytometry analysis. In young animals, the treatment did not affect tumoral CD8+ T cell or Treg numbers (Figure 5C). By contrast, mature mice receiving anti–VLA-4 treatment had significantly reduced tumoral CD8+ T cell numbers (Figure 5C). In both young and mature mice, anti–VLA-4 treatment resulted in smaller CD49d+ populations (Figure 5D and Supplemental Figure 10). A dramatic decrease in the T cell numbers in tumors with anti–VLA-4 treatment indicates that the net effect of anti–VLA-4 treatment is a reduced lymphocyte infiltration into the tissue and consequent reduction of antitumor activity. In fact, we were able to observe a reduced expression level of granzyme B in tumoral CD8+ T cells of mature mice treated with anti-CD49d treatment (Supplemental Figure 11). Overall, these results suggest that VLA-4 expression in CD8+ T cell is protective and required for efficient tumoral control.

Considering that TAMs can promote cancer growth, we wondered whether enhanced tumor progression triggered by anti–VLA-4 antibody treatment in mature mice could be caused, at least in part, by an increased number of TAMs. However, we found that anti–VLA-4 antibody instead moderately decreased the number of TAMs (Supplemental Figure 12). Also, anti–VLA-4 antibody treatment did not substantially alter the number of tumor-infiltrating DCs and neutrophils (Supplemental Figure 12).

Discussion

Aging affects nearly every component of the immune system. Collectively, these immunosenescence changes manifest as increased susceptibility to infections and the age-related occurrence of cancer (27, 28). While our understanding of immunosenescence has progressed over the last decades, many of the underlying mechanisms are still incompletely understood. Importantly, it is often unclear which changes are causes and which are consequences. Gaining deeper, system-wide knowledge of this biology will be critical in combating age-related immune system decline and using this knowledge to better harness the immune system in immunotherapy. The complex, highly adaptive immune system functionally interacts with several other systems within the organism (e.g., neuro/endocrine/immune axis). Given these complexities, we set out to investigate a well-established model system of age-dependent tumor growth in mice to determine how immune cell numbers and functions might control tumor growth.

Our results show that tumors in young mice (a) grow at a much faster rate; (b) contain far fewer tumoral CD8+ cells; and (c) contain tumoral lymphocytes with much lower ITGA4 levels compared with those from mature mice, and ITGA4^hi CD8+ T cells exhibit greater cytolytic effector potential. These results demonstrate that ITGA4^hiCD8+ T cells have an antitumor, protective effect. Further, these data elicit a number of questions: (a) Why do young mice have less ITGA4 on tumor-infiltrating CD8; (b) how does

ITGA4 expression affect the effector function of CD8+ T cells in tumor tissues; (c) can ITGA4 expression be upregulated pharmacologically; and (d) what is the human relevance of these observations?

It has been documented that central memory (CD44+CD62L+) CD8+ T cells accumulate with aging in both human and mice (29). Furthermore, many of these cell are so-called virtual memory cells, as they develop through homeostatic expansion without antigenic stimulation (29, 30). Interestingly, it has been reported that true central memory CD8+ T cells that develop after antigenic stimulation not only upregulate expression of CD44, but also CD49d, where as virtual memory T cells do not upregulate CD49d (31–33). In our study, we do see the trend of increased central memory CD8+ T cell population in tissues of mature mice, including tumor, peripheral blood, spleens, and lymph nodes (data not shown). However, a relatively small fraction of tumor-infiltrating CD8+ T cells was central memory T cells (13.9% ± 2.5% in mature mice and 3.1% ± 0.2% in young mice), and these cells still expressed a substantial level of CD49d (9.6% ± 3.1%), exhibiting the phenotype of antigenic stimulation.

Considering the apparent protective effect of ITGA4, it is tempting to speculate that pharmaceutical manipulation could be performed to upregulate ITGA4 expression levels in young mice. Although we did not perform such experiments due to the lack of well-established systemically administrable agonists, there are some possibilities. For example, a recent study has described the first VLA-4 agonist (THI0019), which was derived from an antagonist and tested in cell culture (34). This study showed activation of VLA-4 enhances T cell adhesion in culture by facilitating the rolling and spreading of cells on VCAM-1 and the migration of cells toward chemoattractant. The intent of the development was to activate the cell adhesion receptors to improve retention and engraftment progenitor cells in stem cell–based therapies. Another way to enhance ITGA4 expression could be via canonical pathways. For example, TLR4 activation reportedly elevates ITGA4 in monocytes (35). In that study, LPS stimulation induced association of MAIR-II with FcRγ chain and Syk, leading to enhancement of ITGA4-mediated adhesion to VCAM-1. Whether similar possibilities exist in lymphocytes, which have much lower TLR expression levels, remains unclear.

The results obtained in this study may have several translational implications. First, more extensive studies are needed to determine whether ITGA levels play a role in human tumoral control. Given the strong evidence in mouse models (and the therapeutic effects of VLA-4 modulation), such studies are warranted. Perhaps the simplest type of study would be to compare ITGA4 expression levels in responders and nonresponders and determine whether ITGA4 levels have prognostic values. Currently available data are inconclusive, pointing to unfavorable prognosis in renal cell cancer and favorable prognosis in head and neck cancers (36). More challenging studies might stimulate ITGA4 during T cell therapies (37). Finally, if ITGA4 shows promise as a pharmacological target, it could lead to new classes of agonists, perhaps even targeting lymphocytes. Irrespective of the therapeutic human implications, this study shows how aging affects tumor microenvironment immune cells, suggesting that host age is a factor to be recognized in preclinical and clinical testing of antitumor therapies.

Methods

Animal studies. All mouse studies were performed using male and female mice of C57BL/6 background purchased from Jackson Laboratory, unless otherwise indicated. Experiments were initiated when animals reached at least 10 weeks of age for the young group and 12 months of age for mature group. Unless otherwise noted, young mice were 2–3 months of age and mature mice were 12–15 months of age at the time of tissue harvest for data collection. Prior to all tumor implantations, mice were anesthetized using 2% isoflurane in oxygen, and hair was removed. S.c. tumor cell implantation was performed using $1 × 10^6$ cells resuspended in 50 μl of sterile PBS per inoculation. Tumor growth was monitored by caliper measurement, and tumor volume (V) was calculated using the formula $V = (\pi × L × W^2)/6$, where L is the largest tumor diameter and W is the perpendicular tumor diameter. For anti-CD8 and anti–VLA-4 antibody treatments, mice were given 25 μg of the anti-CD8 antibody (clone 53-6.7, Bio X Cell) and anti–VLA-4 antibody (clone PS/2, Bio X Cell) per g body weight via i.p. injection. Tumors were harvested between days 10–14 unless otherwise indicated.

Tumor models. Cells were maintained in culture at 37°C and 5% CO_2 and screened each month for mycoplasma. MC38 mouse colon carcinoma cells were provided by Mark Smyth (QIMR Berghofer Medical Research Institute). The 4T1 and B16 lines were purchased from ATCC. Both cell lines were cultured in Iscove's Modified Dulbecco's Medium supplemented with 10% heat-inactivated FCS, 100 IU penicillin, and 100 μg/ml streptomycin (Invitrogen). Cell lines were passaged every 2–3 days to keep cells under 80% confluency.

Intracellular staining. Cells were fixed with 4% paraformaldehyde after cell surface marker staining and stained with anti-FoxP3 antibody (clone MF-14, BioLegend), anti–granzyme B antibody (clone GB11, BioLegend), or anti–IFN-γ antibody (clone XMG1.2, BioLegend) for 30 minutes in permeabilization buffer (TrueNuclear kit, BioLegend). For IFN-γ staining, CD8+ T cells isolated from tumors were restimulated with PMA and ionomycin in the presence of Brefeldin A for 4 hours at 37°C before fixing. For Ki-67 staining, cells were fixed and permeabilized with cold 70%–80% ethanol, and incubate at –20°C for at least 2 hours. After 2 washes in staining buffer (HBSS containing 2% FBS), cells were stained with anti–Ki-67 antibody (clone 16A8, BioLegend) for 30 minutes at room temperature in the dark.

Flow cytometry. Tumors and spleens were excised and cut into small pieces and subsequently digested using collagenase type i, collagenase type iv, and DNase I (Worthington) in HBSS for 25 minutes at 37°C. Digests were passed through a 70-μm cell strainer, washed with HBSS with 2% FBS, and stained for flow cytometry. Samples were first incubated with True Stain FcX antibody (BioLegend) to block Fc receptors. PE-Cy7–conjugated anti-CD45 (clone 30-F11), APC-Cy7–conjugated anti-CD8 (clone 53-6.7), APC-conjugated anti-CD11c (clone N418), Brilliant Violet 510–conjugated anti-CD11b (clone M1/70), APC-conjugated anti-F4/80 (clone BM8), Pacific Blue–conjugated anti-MHC II (clone M5/114.15.2), Alexa 700–conjugated anti-CD25 (clone PC61), Alexa 488–conjugated anti-FoxP3 (clone MF-14), and PE-conjugated anti-CD49d (clone R1-2) were purchased from BioLegend. Brilliant Violet 650–conjugated anti-CD4 (clone GK1.5) was purchased from BD Biosciences. Cells were stained for 30 minutes in HBSS containing 2% FBS and 2 mM EDTA. Propidium iodide or Zombie UV (BioLegend) was used to exclude dead cells. Cells were washed and filtered after staining and were then run on a BD LSRII flow cytometer or BD AriaII for cell sorting. Flow cytometry data were then analyzed using FlowJo software (Tree Star Inc.).

RNA-seq analysis. To prepare RNA-seq samples, 1,000 CD8+, CD4+, or Treg cells from digested tumor tissues or spleens of young and mature mice were double-sorted into Eppendorf tubes containing 5 μl of TCL buffer (Qiagen) with 1% 2-mercaptoethanol and frozen immediately on dry ice. Collected cells were processed for RNA extraction and RNA-seq analysis as per Ultra-low-input RNA-seq protocol provided by Immunological Genome Project (https://www.immgen.org/Protocols/ImmGenULI_RNAseq_methods.pdf). Briefly, total RNA was purified on RNAClean XP beads (Beckman Coulter). Polyadenylated mRNA was then selected using an anchored oligo(dT) primer and converted to cDNA. First-strand cDNA was subjected to limited PCR amplification followed by Tn5 transposon based fragmentation using the Nextera XT DNA Library Preparation Kit (Illumina). Samples were then PCR amplified for 18 cycles using barcoded primers such that each sample carried a specific combination of 8 base Illumina P5 and P7 barcodes and were pooled together prior to SMART sequencing (SMART-seq). SMART-seq paired-end sequencing was performed on an Illumina NextSeq500 using 2 × 25 bp reads with no further trimming. Reads were aligned to the mouse genome (GENCODE GRCm38/mm10 primary assembly and gene annotations vM16; https://www.gencodegenes.org/mouse/release_M16.html with STAR 2.5.4a (https://github.com/alexdobin/STAR/releases). The ribosomal RNA gene annotations were removed from General Transfer Format (GTF) file. The gene-level quantification was calculated by featureCounts (http://subread.sourceforge.net/). Raw reads counts tables were normalized by median of ratios method with DESeq2 package version 1.18.1. from Bioconductor (https://bioconductor.org/packages/release/bioc/html/DESeq2.html, ref. 38). Samples with less than 1 million uniquely mapped reads were automatically excluded from normalization to mitigate the effect of poor-quality samples on normalized counts. Differentially expressed genes in samples from young and mature mice were selected with Benjamini-Hochberg adjusted P value (FDR) < 0.05. Data analysis was performed in R version 3.4.3. The sequencing data presented in this study was submitted to the Gene Expression Omnibus (GEO) under accession number GSE121075. A complete R markdown document detailing all analyses is provided in the Supplemental Methods.

Statistics. Data points were compiled in Microsoft Excel, and statistical analyses were performed using GraphPad Prism 7. Statistical tests used to calculate P values for each figure are indicated in the figure legends. Mann-Whitney U test was used for statistical analysis of tumor growth data in Figures 1, 2 and 5. Two-tailed t test with correction for multiple comparisons by Holm-Sidak was used for cell counts and flow cytometry results in Figures 2, 3, 4, and Table 1. Two-way ANOVA was used for Figure 5D. $P < 0.05$ was used to define statistical significance. Unless otherwise noticed, all data are plotted as means ± SEM. All presented data are from at least 3 repeated experiments.

Study approval. All animal studies were performed in accordance with the guidelines established by the IACUC at MGH.

Author contributions

JO, MJP, and RW developed the concepts and designed the experiments. JO performed all experiments and analyzed the data. AM and JO performed and analyzed RNA-seq results under CB's supervision. JO and RW wrote the manuscript. All authors analyzed results and reviewed and edited the manuscript.

1. Leading Cancer Cases and Deaths, Male and Female, 2015. U.S. Department of Health and Human Services, Centers for Disease Control and Prevention and National Cancer Institute. https://gis.cdc.gov/Cancer/USCS/DataViz.html. Accessed Ocotber 29, 2018.
2. Ershler WB, Stewart JA, Hacker MP, Moore AL, Tindle BH. B16 murine melanoma and aging: slower growth and longer survival in old mice. *J Natl Cancer Inst*. 1984;72(1):161–164.
3. Kreisle RA, Stebler BA, Ershler WB. Effect of host age on tumor-associated angiogenesis in mice. *J Natl Cancer Inst*. 1990;82(1):44–47.
4. Pili R, Guo Y, Chang J, Nakanishi H, Martin GR, Passaniti A. Altered angiogenesis underlying age-dependent changes in tumor growth. *J Natl Cancer Inst*. 1994;86(17):1303–1314.
5. Ershler WB, Socinski MA, Greene CJ. Bronchogenic cancer, metastases, and aging. *J Am Geriatr Soc*. 1983;31(11):673–676.
6. Fisher CJ, Egan MK, Smith P, Wicks K, Millis RR, Fentiman IS. Histopathology of breast cancer in relation to age. *Br J Cancer*. 1997;75(4):593–596.
7. Calabrese CT, Adam YG, Volk H. Geriatric colon cancer. *Am J Surg*. 1973;125(2):181–184.
8. Itzhaki O, et al. Age-adjusted antitumoral therapy based on the demonstration of increased apoptosis as a mechanism underlying the reduced malignancy of tumors in the aged. *Biochim Biophys Acta*. 2004;1688(2):145–159.
9. Ershler WB, Moore AL, Shore H, Gamelli RL. Transfer of age-associated restrained tumor growth in mice by old-to-young bone marrow transplantation. *Cancer Res*. 1984;44(12 pt 1):5677–5680.
10. Nikolich-Žugich J. The twilight of immunity: emerging concepts in aging of the immune system. *Nat Immunol*. 2018;19(1):10–19.
11. Jagger A, Shimojima Y, Goronzy JJ, Weyand CM. Regulatory T cells and the immune aging process: a mini-review. *Gerontology*. 2014;60(2):130–137.
12. Jackaman C, et al. Aging and cancer: The role of macrophages and neutrophils. *Ageing Res Rev*. 2017;36:105–116.
13. Goronzy JJ, Lee WW, Weyand CM. Aging and T-cell diversity. *Exp Gerontol*. 2007;42(5):400–406.
14. Goronzy JJ, Weyand CM. Successful and maladaptive T cell aging. *Immunity*. 2017;46(3):364–378.
15. Arnold, et al. Gain and loss of T cell subsets in old age--age-related reshaping of the T cell repertoire. *J Clin Immunol*. 2011;31(2):137–146.
16. Mosely SI, et al. Rational selection of syngeneic preclinical tumor models for immunotherapeutic drug discovery. *Cancer Immunol Res*. 2017;5(1):29–41.
17. Siegel RL, Miller KD, Jemal A. Cancer Statistics, 2017. *CA Cancer J Clin*. 2017;67(1):7–30.
18. Fox JG, Barthold S, Davisson M, Newcomer C, Quimby F, Smith A. *The Mouse in Biomedical Research*. Vol. 2. 2nd ed. Burlington, Massachusetts, USA: Academic Press; 2007.
19. Belsky, et al. Quantification of biological aging in young adults. *Proc Natl Acad Sci U S A*. 2015;112(30):E4104–E4110.
20. Sun Y, Li H, Langnas AN, Zhao Y. Altered allogeneic immune responses in middle-aged mice. *Cell Mol Immunol*. 2004;1(6):440–446.
21. Sinke AP, et al. Genetic analysis of mouse strains with variable serum sodium concentrations identifies the Nalcn sodium channel as a novel player in osmoregulation. *Physiol Genomics*. 2011;43(5):265–270.
22. Xing S, et al. Genetic influence on electrocardiogram time intervals and heart rate in aging mice. *Am J Physiol Heart Circ Physiol*. 2009;296(6):H1907–H1913.
23. Champy MF, et al. Genetic background determines metabolic phenotypes in the mouse. *Mamm Genome*. 2008;19(5):318–331.
24. Pettan-Brewer C, Morton J, Coil R, Hopkins H, Fatemie S, Ladiges W. B16 melanoma tumor growth is delayed in mice in an age-dependent manner. *Pathobiol Aging Age Relat Dis*. 2012;2.
25. Miller DH, et al. A controlled trial of natalizumab for relapsing multiple sclerosis. *N Engl J Med*. 2003;348(1):15–23.
26. Polman CH, et al. A randomized, placebo-controlled trial of natalizumab for relapsing multiple sclerosis. *N Engl J Med*. 2006;354(9):899–910.
27. Foster AD, Sivarapatna A, Gress RE. The aging immune system and its relationship with cancer. *Aging Health*. 2011;7(5):707–718.
28. Gruver AL, Hudson LL, Sempowski GD. Immunosenescence of ageing. *J Pathol*. 2007;211(2):144–156.
29. Nikolich-Zugich J. Ageing and life-long maintenance of T-cell subsets in the face of latent persistent infections. *Nat Rev Immunol*. 2008;8(7):512–522.
30. Rudd BD, et al. Nonrandom attrition of the naive CD8$^+$ T-cell pool with aging governed by T-cell receptor:pMHC interactions. *Proc Natl Acad Sci U S A*. 2011;108(33):13694–13699.
31. Chiu BC, Martin BE, Stolberg VR, Chensue SW. Cutting edge: central memory CD8 T cells in aged mice are virtual memory cells. *J Immunol*. 2013;191(12):5793–5796.

32. Akue AD, Lee JY, Jameson SC. Derivation and maintenance of virtual memory CD8 T cells. *J Immunol*. 2012;188(6):2516–2523.

33. Haluszczak C, et al. The antigen-specific CD8+ T cell repertoire in unimmunized mice includes memory phenotype cells bearing markers of homeostatic expansion. *J Exp Med*. 2009;206(2):435–448.

34. Vanderslice P, et al. Small molecule agonist of very late antigen-4 (VLA-4) integrin induces progenitor cell adhesion. *J Biol Chem*. 2013;288(27):19414–19428.

35. Totsuka N, et al. Toll-like receptor 4 and MAIR-II/CLM-4/LMIR2 immunoreceptor regulate VLA-4-mediated inflammatory monocyte migration. *Nat Commun*. 2014;5:4710.

36. Ulhen M, et al. A pathology atlas of the human cancer transcriptome. *Science*. 2017;357(6352):eaan2507.

37. Kalos M. CART Targeting of solid tumors: more pieces to the puzzle. *Clin Cancer Res*. 2018;24(6):1246–1247.

38. Love MI, Huber W, Anders S. Moderated estimation of fold change and dispersion for RNA-seq data with DESeq2. *Genome Biol*. 2014;15(12):550.